Semi-Automatic Basket Catheter Reconstruction from two X-ray views

X. Zhong[1], M. Hoffmann[1], N. Strobel[2], and A. Maier[1,3]

[1] Pattern Recognition Lab, Friedrich-Alexander-Universität Erlangen-Nürnberg, Erlangen, Germany,
[2] Siemens Healthcare GmbH, Forchheim, Germany,
[3] Erlangen Graduate School in Advanced Optical Technologies (SAOT)

Abstract. Ablation guided by focal impulse and rotor mapping (FIRM) is a novel treatment option for atrial fibrillation, a frequent heart arrhythmia. This procedure is performed minimally invasively and at least partially under fluoroscopic guidance. It involves a basket catheter comprising 64 electrodes. The 3-D position of these electrodes is important during treatment. We propose a novel model-based method for 3-D reconstruction of this catheter using two X-ray images taken from different views. Our approach requires only little user interaction. An evaluation of the method found that the electrodes of the basket catheter can be reconstructed with a median error of 1.5 mm for phantom data and 3.4 mm for clinical data.

1 Introduction

Atrial (Afib) fibrillation is one of the most common heart arrhythmia. In particular, for persistent Afib, ablation guided by focal impulse and rotor mapping (FIRM) has been proposed as an alternative to traditional treatment options [11]. To perform a FIRM-based ablation procedure, a multielectrode basket catheter is placed first in the right atrium and then into left atrium during the case. The basket catheter's shape resembles an ellipsoid when imaged under X-ray (see Fig. 1). It has eight splines, each spline comprising eight electrodes. One marker electrode can be identified by its larger size. The catheter is used to record the electrical signals in the atria. Using the Topera RhythmView 3-D electrophysiological mapping system (Topera Inc., Palo Alto, CA, USA), the position of electrical anomalies, so-called rotors can be found. This position is determined relative to the splines and the electrode positions of the basket catheter and indicates endocardial substrate maintaining the arrhythmia, that may be ablated. A method is required to remap the rotor position from its basket catheter-based coordinate system to the anatomical positions in the left and right atrium.

As of now, remapping and associated catheter navigation is performed using the EnSite Velocity mapping system (St. Jude Medical, St. Paul, MN, USA). However, the use of the EnSite system is problematic for at least two reasons. First, current healthcare economics leave very little financial room to use a second mapping system during an Afib ablation procedure. Second, it is known

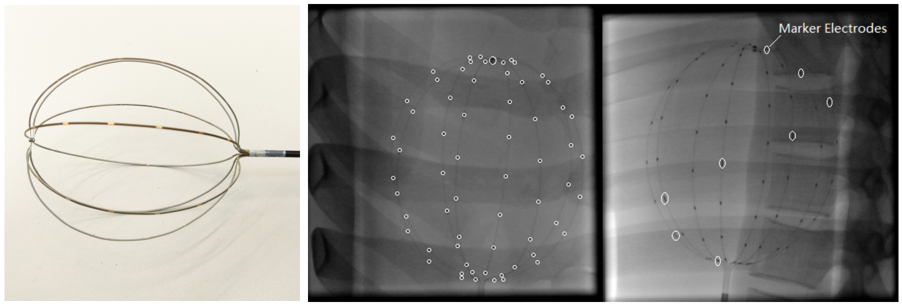

Fig. 1: Basket catheter, displayed left, as seen in two X-ray views taken from different directions. The basket catheter comprises eight splines carrying eight electrodes. Each spline has a marker electrode highlighted with ellipses (right).

that an impedance-based localization system such as Ensite Velocity may suffer from electrical field distortions [6]. As an alternative to the mapping system, we propose a method based on two X-ray images taken from different directions to detect and reconstruct the basket catheter in 3-D. This is a challenging task as the catheter is usually deformed by the atria. This results in a complex structure compared with other electrophysiological catheters such as the coronary sinus catheter and the circumferential mapping catheter [9].

1.1 Related Work

Image based 3-D catheter detection or reconstruction methods require usually the detection of features, e.g., the center line or electrodes of the catheter. The 3-D catheter can then either be generated bottom up from these features, or, in a top-down manner, i.e., an an initialization of 3-D curve can be approximated towards the features. Hoffman et al. [9] proposed to use a bottom up strategy which detects the center line of a catheter in two different views first. Then it uses epipolar geometry to reconstruct an 3-D point cloud. They also proposed a method to find the correct order of a subset of points in the point cloud to reconstruct the catheter. Using 3-D curve segments as the feature rather than a 3-D point cloud, Delmas et al. [5] proposed a method to estimated the optimal ordered subset of 3-D curve segments and applied constraints to reconstruct the catheter. Using top-down strategy, Mauri [3] proposed a method using B-snakes to formulate the catheter detection and reconstruction as an energy minimization problem. Unfortunately, none of these approaches can be applied to our problem as the basket catheter has a complex structure. Furthermore, it is not always possible to extract the basket catheter splines as the contrast can be very low.

We present a top-down approach to reconstruct the shape of a basket catheter in 3-D using two 2-D X-ray images acquired from different directions. For reconstruction of the rather complex structure of the basket catheter, we propose to use a statistical shape model. The model is adapted to the electrodes and wires extracted in two 2-D images. Our method has been designed for the basket catheter, but can inspire reconstruction methods for other complex catheters.

2 Method

The method to detect the basket catheter comprises three steps. In the first step, we train the shape model of the basket catheter based on annotated ground truth data. In the second step, we detect the electrodes and splines of the basket catheter in the X-ray images taken from two different viewing directions. Using these 2-D points, we reconstruct all possible 3-D electrode candidates using triangulation. In this step, the user is is also asked to specify the start and the end of the basket catheter at least one of the marker electrodes. The marker electrodes determine the order of the catheter splines. In the last step, the initialization of the model will be performed and the model will be matched to the extracted features in the 2-D images. A different, possibly more intuitive approach, may have been to assign electrodes to splines followed by 3-D reconstruction. However, it might be difficult to compute this assignment, especially if splines connecting the electrodes are not well visible, and an exhaustive search would possibly take too long to execute in a clinical environment.

2.1 Basket Catheter Spline Model

We describe each single spline of the basket catheter using a statistic shape model [4]. The choice to use a shape model was motivated by the desire to constrain the basket catheter reconstruction problem as much as possible yet being able to use prior knowledge about the expected deformation. The model is trained using the 3-D electrode positions of M splines which origin from several, differently deformed catheters. We combine the basket catheter's start point $\boldsymbol{p}_{i1} \in \mathbb{R}^3$, eight electrodes $\boldsymbol{p}_{i2}, \ldots, \boldsymbol{p}_{i9}$ and the basket's end point $\boldsymbol{p}_{i10}$ of the i^{th} spline in a vector $\boldsymbol{x}_i'$

$$\boldsymbol{x}_i' = \left(\boldsymbol{p}_{i1}^T, \ldots, \boldsymbol{p}_{ik}^T, \ldots, \boldsymbol{p}_{i10}^T\right)^T \tag{1}$$

Such a description is established for each of the M basket catheter splines. To build the statistical shape model, the data needs to be normalized first. The normalization involves a rotation and translation in 3-D, scaling is not necessary, as the size of the catheter is standardized. We normalized the data $\boldsymbol{x}_i'$ so that the start point $\boldsymbol{p}_{i1}$ and the end point $\boldsymbol{p}_{i10}$ lie both on the y-axis. The middle point between these two points is defined as origin. Furthermore, during alignment we make sure that the eight electrodes $\boldsymbol{p}_{i2}, \ldots, \boldsymbol{p}_{i9}$ have minimum distance to the $X-Y$ plane and and that their x-coordinates are positive. So, the alignment for point $\boldsymbol{p}_{ik}$ in i^{th} catheter spline can be formulated as

$$\boldsymbol{x}_{ik} = \mathbf{R}_i^Y \mathbf{R}_i (\boldsymbol{p}_{ik} + \boldsymbol{t}_i) \tag{2}$$

where $\boldsymbol{x}_i = \left(\boldsymbol{x}_{i1}^T, \ldots, \boldsymbol{x}_{i10}^T\right)^T \in \mathbb{R}^{30}$ denotes the normalized and aligned points, $\boldsymbol{t}_i$ and $\mathbf{R}_i$ denote the translation and rotation for normalization, and $\mathbf{R}_i^Y$ denotes the rotation along the Y axis for alignment. Then we follow the steps from Cootes et al. [4], calculate the mean shape $\bar{\boldsymbol{x}}$, the deviation $d\boldsymbol{x}_i$ from the mean and the covariance matrix $\boldsymbol{\Sigma}$ as

$$\bar{\boldsymbol{x}} = \frac{1}{M}\sum_{i=1}^{M}\boldsymbol{x}_i \qquad d\boldsymbol{x}_i = \boldsymbol{x}_i - \bar{\boldsymbol{x}} \qquad \boldsymbol{\Sigma} = \frac{1}{M}\sum_{i=1}^{M} d\boldsymbol{x}_i d\boldsymbol{x}_i^T \tag{3}$$

By calculating an eigenvalue and eigenvector decomposition of the covariance matrix $\boldsymbol{\Sigma}$, we get unit eigenvectors $\boldsymbol{v}_k$ $(k = 1, \ldots, 30)$ with corresponding eigenvalues λ_k in descending order. Using the first N_m modes of variation $\mathbf{V} = (\boldsymbol{v}_1, \ldots, \boldsymbol{v}_{N_\mathrm{m}})$ and the corresponding weight factors $\boldsymbol{b}' = (b_1, \ldots, b_{N_\mathrm{m}})$, we can generate new shapes $\boldsymbol{x}'$ of the model as

$$\boldsymbol{x}' = \bar{\boldsymbol{x}} + \mathbf{V}\boldsymbol{b}' \tag{4}$$

In the remainder of the paper, we use $N_\mathrm{m} = 3$ modes of variations.

2.2 Electrode and Spline Detection

We detect the electrodes in the image $\mathbf{I}(x, y)$ using the determinant of the Hessian matrix $\mathbf{H}$ [10] of a scale space representation

$$\mathbf{L}(x, y; \sigma^2) = \mathbf{I}(x, y) * \mathbf{G}(x, y; \sigma^2) \tag{5}$$

obtained by a convolution with a Gaussian kernel $\mathbf{G}(x, y; \sigma^2)$ of size σ. To detect blobs of different sizes, different values of σ should be chosen. Steger [12] stated that the center point of a bar-shaped profile with a width of $2w$ can be extracted when $\sigma \geq w/\sqrt{3}$. With prior knowledge of electrodes' dimensions w_p and the projection geometry information of the C-arm, we can estimate a minimal scale σ_min. Let m be the perspective magnification factor of the X-ray system and s_p be pixel spacing. Based on the length w_im of the electrode as it appears in the X-ray image (in pixels), we select the scale as

$$\sigma_\mathrm{min} = \frac{w_\mathrm{im}}{2\sqrt{3}} \qquad \text{with} \quad w_\mathrm{im} = \frac{w_\mathrm{p} \cdot m}{s_\mathrm{p}} \tag{6}$$

We use two different scales, σ_min and $2\sigma_\mathrm{min}$, to calculate the determinant of the Hessian matrix for each pixel. Then we apply a threshold on the determinant of the Hessian to obtain an electrode mask image. The threshold level is selected such that a certain percentage of image pixels is extracted as the number of image pixels covered by electrodes is roughly known in advance. We then select the possible positions of the electrodes denoted as $\mathbf{e}_i^\mathrm{A}$ and $\mathbf{e}_i^\mathrm{B}$ in image A and B. Therefore, the local maximum of the determinant of the Hessian in each connected component of the mask image is selected as electrode center. Finally, the user is required to mark the start point $\tilde{\boldsymbol{p}}_1^\mathrm{A}$, $\tilde{\boldsymbol{p}}_1^\mathrm{B}$ and the end point $\tilde{\boldsymbol{p}}_{10}^\mathrm{A}$, $\tilde{\boldsymbol{p}}_{10}^\mathrm{B}$ of the basket catheter by clicking on them in the 2-D images of plane A and B, respectively. Additionally, either one or eight spline marker points are marked in both views. The 3-D position of the start point $\tilde{\boldsymbol{p}}_1$, end point $\tilde{\boldsymbol{p}}_{10}$ and the marker electrode(s) are obtained using triangulation.

2.3 Point Cloud Generation

We use epipolar geometry to search for correspondences between electrodes in associated two-view images. When searching for correspondences, we introduce some margin for acceptance. This acceptance range depends on the X-ray system used. For a bi-plane system, the acceptance range will be only a few pixels to compensate the blob detection error due to limited precision or residual camera calibration error. For mono-plane systems, patient motion might occur between the two acquisitions from different views. Therefore, we accept a higher margin and apply additionally a motion compensation using the marked 2-D catheter start points $\tilde{\boldsymbol{p}}_1^{\mathrm{A}}$, $\tilde{\boldsymbol{p}}_1^{\mathrm{B}}$ and the marked 2-D endpoints $\tilde{\boldsymbol{p}}_{10}^{\mathrm{A}}$, $\tilde{\boldsymbol{p}}_{10}^{\mathrm{B}}$ of image plane A and B, respectively. This motion compensation is applied to the projection matrix $\mathbf{P}^{\mathrm{A}}$ associated with plane A by multiplying it with a 3-D translation matrix $\mathbf{T} = \left(1 \mid (t_x, t_y, t_z)^T\right)$. The $\mathbf{T}$ are selected such that the distance between the projection rays from $\tilde{\boldsymbol{p}}_1^{\mathrm{A}}$ and $\tilde{\boldsymbol{p}}_1^{\mathrm{B}}$ and the distance between the projection rays of $\tilde{\boldsymbol{p}}_{10}^{\mathrm{A}}$ and $\tilde{\boldsymbol{p}}_{10}^{\mathrm{B}}$ is minimal. For each possible point correspondence, a 3-D point is triangulated [8].

Finally, the catheter splines are extracted using a vesselness filter [7, 2]. After applying a threshold, distance maps $\mathbf{I}_{\mathrm{ds}}^{\mathrm{A}}$ and $\mathbf{I}_{\mathrm{ds}}^{\mathrm{B}}$ to the splines in image A and B, respectively, are computed.

2.4 Model Initialization and Adaption

Length Adaption Using the 3-D start point $\tilde{\boldsymbol{p}}_1$ and the end point $\tilde{\boldsymbol{p}}_{10}$ marked by the user, we perform an initialization of all single splines of the basket catheter model. Let $\hat{\boldsymbol{p}}_{k1}(\boldsymbol{b}')$ and $\hat{\boldsymbol{p}}_{k10}(\boldsymbol{b}')$ be the start point and end point of k^{th} spline when using $\boldsymbol{b}'$ as parameters. We select the parameter vector $\boldsymbol{b}_k = (b_{k1}, b_{k2}, b_{k3})^T$ of the k^{th} spline such that $\|\tilde{\boldsymbol{p}}_1 - \tilde{\boldsymbol{p}}_{10}\| = \|\hat{\boldsymbol{p}}_1(\boldsymbol{b}') - \hat{\boldsymbol{p}}_{10}(\boldsymbol{b}')\|$. As this is an under-termined problem, we propose two different ways of adding constraints. One is called most probable model which is estimated by optimizing following equation

$$\boldsymbol{b}_k = \underset{\boldsymbol{b}'}{\operatorname{argmin}} \|\tilde{\boldsymbol{p}}_1 - \tilde{\boldsymbol{p}}_{10}\| - \|\hat{\boldsymbol{p}}_1(\boldsymbol{b}') - \hat{\boldsymbol{p}}_{10}(\boldsymbol{b}')\| - a_0 \cdot \mathcal{N}(\boldsymbol{b}'; \mathbf{0}, \boldsymbol{\Sigma}) \tag{7}$$

For the second approach, we manually define a set of different ratios between b_{k1}, b_{k2} and b_{k3}. With these extra constraints, the problem becomes determined and can be solved. We use these parameters for all eight splines and distribute them with equal angle spacing around the axis defined by the start point $\tilde{\boldsymbol{p}}_1$ and the end point $\tilde{\boldsymbol{p}}_{10}$ to get a model of the whole basket catheter. As shown in Fig. 5, the shape of the model can be very different subject to the same start and end point.

Rotation Initialization Starting with this initial model, we also need to estimate the rotation $\boldsymbol{\alpha} = (\alpha_1, \ldots, \alpha_8)$ of each single spline. In case we have eight marker electrodes as input, the rotation for all single splines is computed such that their distance to their respective marker electrode is minimal. With one

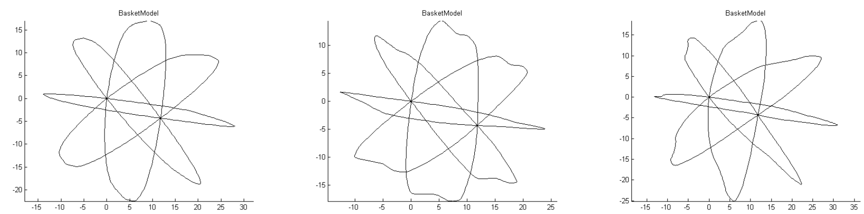

Fig. 2: Different possible shapes with same start point $\tilde{\boldsymbol{p}}_1$ and end point $\tilde{\boldsymbol{p}}_{10}$

marker electrode input, the whole basket catheter is rotated such that the distance of the marker electrode to its respective spline is minimal. Based on the result, we estimate further the rotation of the other remaining splines. We define therefore an energy-term $\mathcal{D}$ to describe the difference between the projected model and the extracted features in both images as

$$\begin{aligned}
\mathcal{D}(\mathbf{b}, \boldsymbol{\alpha}) = a_1 \cdot & \underbrace{\left(\sum_i \min_k d\left(\boldsymbol{e}_i^{\mathrm{A}}, \mathbf{S}_k^{\mathrm{A}}(\boldsymbol{b}_k, \alpha_k)\right) + \sum_i \min_k d\left(\boldsymbol{e}_i^{\mathrm{B}}, \mathbf{S}_k^{\mathrm{B}}(\boldsymbol{b}_k, \alpha_k)\right) \right)}_{\text{Distance of each detected electrode to projected splines of the model}} \\
a_2 \cdot & \underbrace{\left(\sum_i \min_{j,k} d\left(\boldsymbol{e}_i^{\mathrm{A}}, \boldsymbol{p}_{k,j}^{\mathrm{A}}(\boldsymbol{b}_k, \alpha_k)\right) + \sum_i \min_{j,k} d\left(\boldsymbol{e}_i^{\mathrm{B}}, \boldsymbol{p}_{k,j}^{\mathrm{B}}(\boldsymbol{b}_k, \alpha_k)\right) \right)}_{\text{Distance of each detected electrode to projected electrodes of the model}} \\
a_3 \cdot & \underbrace{\left(\sum_{k,j} \min_i d\left(\boldsymbol{e}_i^{\mathrm{A}}, \boldsymbol{p}_{k,j}^{\mathrm{A}}(\boldsymbol{b}_k, \alpha_k)\right) + \sum_{k,j} \min_i d\left(\boldsymbol{e}_i^{\mathrm{B}}, \boldsymbol{p}_{k,j}^{\mathrm{B}}(\boldsymbol{b}_k, \alpha_k)\right) \right)}_{\text{Distance of each projected electrode of the model to detected electrodes}}
\end{aligned} \tag{8}$$

where $\boldsymbol{p}_{kj}^{\mathrm{A}} \in \mathbb{R}^2$ denotes the projection of the j^{th} electrode on the k^{th} spline in the image A. The projection of the complete k^{th} 3-D spline in image A is denoted as $\mathbf{S}_k^{\mathrm{A}}$. Their projections in image B are denoted by $\boldsymbol{p}_{k,j}^{\mathrm{B}}$ and $\mathbf{S}_k^{\mathrm{A}}$, respectively. The rotation is estimated by minimizing the energy $\mathcal{D}$

$$\boldsymbol{\alpha} = \operatorname*{argmin}_{\alpha_1,\ldots,\alpha_8} \mathcal{D}(\mathbf{b}, \alpha_1, \ldots, \alpha_8) \tag{9}$$

Outlier Reduction The initialization described at the beginning of this section assumes that the basket catheter is symmetrical, i.e. the parameter vector $\boldsymbol{b}_k$ is the same for each spline. To cover also asymmetrical cases, we will use the 3-D electrode point cloud to adapt the initialization. As we have potentially many outliers in the 3-D point cloud, we will perform an iterative outlier reduction and model estimation algorithm. This Algorithm, which is described in Algo. 1, assigns 2-D electrodes to 3-D splines to detect and eliminate spurious correspondences.

Algorithm 1 Iterative Outlier Reduction and Model Estimation

```
Compute for all electrodes e_i^A detected in image plane A the set C(e_i^A) of corresponding electrodes in image B
for each iteration step t = 1 : N do
    for each e_i^A do
        find the two splines S_t^1, S_t^2 for which their projection S_t^{1A}, S_t^{2A} in image A is closest to e_i^A
        compute their projections S_t^{1B}, S_t^{2B} in image B
        delete from C(e_i^A) the point c_k which maximizes min(d(c_k, S_t^{1B}), d(c_k, S_t^{2B}))
    end for
    reconstruct a new 3-D point cloud using the remaining correspondences
    estimate the model M_t with respect to the new point cloud
    estimate the rotation α_t
end for
```

Image-based Model Adaption Finally, we adapt the model such that it fits to both images by altering the weighting $\boldsymbol{b} = (\boldsymbol{b}_1^T, \ldots, \boldsymbol{b}_k^T)$ and rotation $\boldsymbol{\alpha} = (\alpha_1, \ldots, \alpha_8)$. We introduce therefore an additional energy term

$$\mathcal{R}(\boldsymbol{b}, \boldsymbol{\alpha}) = \underbrace{a_4 \cdot \sum_k \mathcal{N}(\boldsymbol{b}_k; \mathbf{0}, \boldsymbol{\Sigma})}_{\text{Model likelyhood}} + a_5 \cdot \underbrace{\sum_k \mathbf{I}_{\mathrm{ds}}^{\mathrm{A}}(\mathbf{S}_k^{\mathrm{A}}(\boldsymbol{b}_k, \alpha_k)) + \mathbf{I}_{\mathrm{ds}}^{\mathrm{B}}(\mathbf{S}_k^{\mathrm{B}}(\boldsymbol{b}_k, \alpha_k))}_{\text{Distance of projected splines to detected 2-D splines}} \tag{10}$$

for the final optimization of $\boldsymbol{b}$ and the rotation $\boldsymbol{\alpha}$

$$\boldsymbol{b}, \boldsymbol{\alpha} = \operatorname*{argmin}_{\boldsymbol{b}, \boldsymbol{\alpha}} \mathcal{D}(\boldsymbol{b}, \boldsymbol{\alpha}) + \mathcal{R}(\boldsymbol{b}, \boldsymbol{\alpha}) \tag{11}$$

3 Evaluation and Results

For evaluation, we used three different setups. In the first case, the basket catheter was deformed by tape and put into a bottle. A total of 18 different experiments were performed by inserting the basket catheter such that it assumed a different shape each time. Then, a C-arm CT was acquired. As a result, 18 3-D volumes were generated, each containing a differently deformed basket catheter. Also, a series of associated X-ray images taken from different angles was acquired for each volume. In each of the 18 volumes, the positions of the 3-D electrodes were annotated and served as ground truth. For evaluation, two X-ray images, taken from perpendicular view directions, were selected for each of the 18 basket catheter placements. They were taken as the input for our algorithm.

For the second setup, the catheter was placed into a thorax phantom. Then we took four bi-plane image pairs with perpendicular viewing angles at different dose settings. Unlike in the previous experiment, in this case the basket catheter was identically deformed. We used this set to evaluate the performance of our approach with respect to different noise levels.

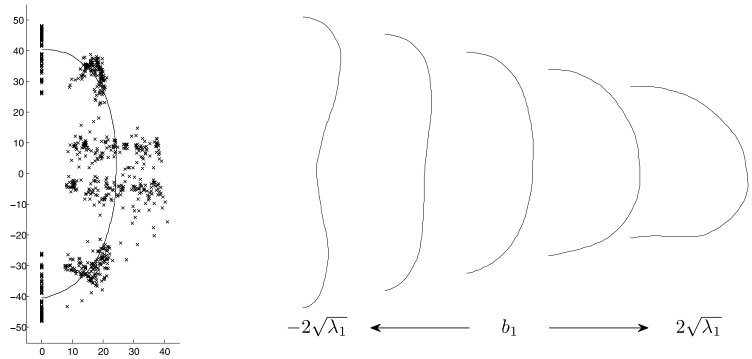

Fig. 3: The coordinates of a subset of the annotated electrodes, normalized and aligned with mean shape of the basket catheter spline model (shown left) and the first mode of variation (displayed right). As most of the variation spreads in the X-Y plane, we projected the mean shape and the variation of the basket into the X-Y plane.

We also included one clinical data set in the evaluation taken from a mono-plane system. Here, the basket was placed in the right atrium along with other electrophysiological catheters. The ground truth positions of the electrodes of the basket catheter were obtained, both for the bi-plane setup and the clinical data, by triangulation of annotated electrodes in both views.

3.1 Result of the Spline Model Training

For training of the basket catheter model, we used the 3-D electrode coordinates annotated from the C-arm CT data sets. For evaluation using the C-arm CT data set, a leave-one-out crossvalidation was performed. The resulting model and the first mode of variation is shown in Fig. 3.

3.2 Basket Catheter Reconstruction Results

C-arm CT Data Set The results of the evaluation using the C-arm CT data sets are shown in Fig. 4. We also investigated how marking all instead of a single spline marker electrode and outlier reduction changed our outcomes. We found that the median error was between 1.7 mm and 1.5 mm. The maximum errors are 24.2 mm and 32.2 mm for single marker annotation without and with outlier reduction, respectively. The respective maximum errors when all markers are annotated are 15.3 mm 24.1 mm. However, we did also encounter outliers of up to 32.2 mm depending on the kind of information provided by the user. Comparing different user interactions, we see that the result improved somewhat when the positions of the eight marker electrodes were provided. Unfortunately, the improvements were limited, both for knowing all marker electrodes and also when applying outlier reduction methods.

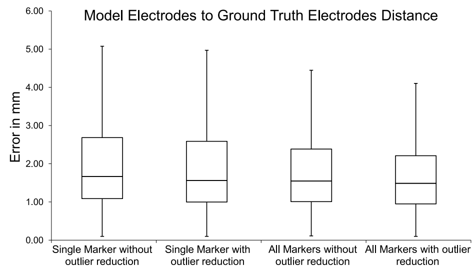

Fig. 4: Evaluation result of C-arm CT data with different electrode selection strategies. The median errors are 1.7 mm and 1.6 mm for single marker annotation without and with outlier reduction, respectively. The respective median errors when all markers are annotated are 1.6 mm 1.5 mm. Results with an error of a 1.5 inter-quartile range above the median error are not shown in the figure.

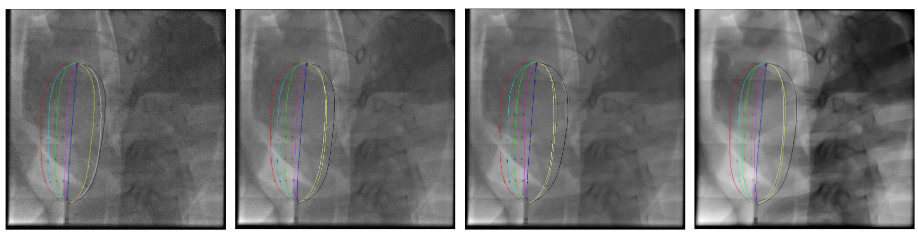

Fig. 5: Images of basket catheter in phantom and overlay of the reconstructed basket catheter. The X-ray dose and image quality improved from left to right.

Bi-plane Views with different X-ray Dose Figure 5 shows qualitative results using images from the bi-plane data set, quantitative results are presented in Figure 6. The result shown in Fig. 6 indicate that our method performed better as the signal to noise ratio improved, i.e., as the X-ray dose was increased. This experiment shows that our method can also perform well at a low SNR.

Clinical Data In Fig. 7, we show the clinical data with the basket catheter in the right atrium. In this case, we used single marker selection without outlier reduction. The result is also shown in this figure. With our method, we reached a median error of 3.4 mm and a maximum error of 12.5 mm, respectively.

4 Discussion and Conclusion

When comparing a 3-D representation of a basket catheter computed by our method from two views to its counterpart generated using C-arm CT, we found a median error below the clinical important threshold of 3mm [1]. Unfortunately, we also encountered large maximum errors. They were caused by heavily deformed and twisted basket catheters in the data set, these cases are not very

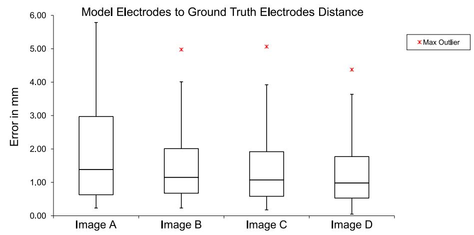

Fig. 6: Evaluation result with biplane X-ray data acquired at different dose levels. Image A has the poorest SNR, image D has the best SNR.

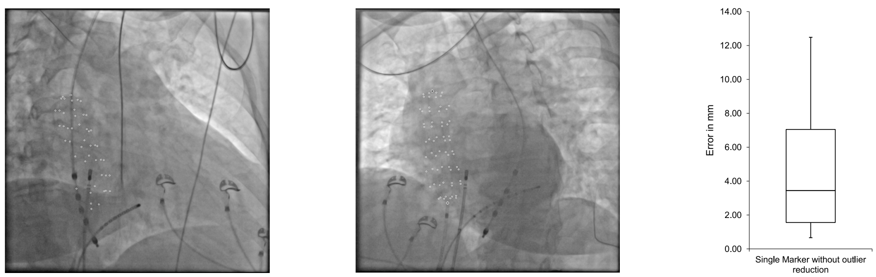

Fig. 7: Left anterior oblique (LAO) 45° view and right anterior oblique (RAO) 30° view of the basket catheter in the right atrium.

clinically relevant as the basket catheters would need to be repositioned in such a situation to obtain a signal reading that can then be reliably processed further. The performance of outlier reduction is also restricted as in some case, some of the electrodes are positioned where multiple splines cross. In such a case, it is also hard for the algorithm to decide which spline the electrode should be assigned to. This problem could be approached by using a consensus based method in the future. In the clinical data set, however, the result was less satisfactory with a median error of 3.4 mm. This error is the consequence of very low-dose data acquisition resulting in X-ray images with a low SNR. In such a situation our electrode detection algorithm identifies many potential electrode positions which do not belong to the basket catheter. Any overlap of the basket catheter with other catheters is also problematic. In such a case, some electrodes of the basket catheter might not be visible and additional electrodes may be introduced that are not associated with the basket catheter. More work on robust basket electrode detection is needed to improve the result. Furthermore, the outlier reduction algorithm should be extended to assign e.g. probabilities to point correspondences. This which might also improve the result.

Acknowledgments. We gratefully acknowledge the feedback by the Klinikum Coburg, Germany, and would also like to thank them for the test images. This work was supported by Siemens Healthcare. The concepts and information presented in this paper are based on research, and are not commercially available.

References

1. Bourier, F., Fahrig, R., Wang, P., Santangeli, P., Kurzidim, K., Strobel, N., Moore, T., Hinkel, C., Amin, A.A.: Accuracy assessment of catheter guidance technology in electrophysiology procedures. Journal of Cardiovascular Electrophysiology 25(1), 74–83 (2014)
2. Budai, A., Bock, R., Maier, A., Hornegger, J., Michelson, G.: Robust Vessel Segmentation in Fundus Images. International Journal of Biomedical Imaging 2013 (2013)
3. Canero, C., Radeva, P., Toledo, R., Villanueva, J., Mauri, J.: 3d curve reconstruction by biplane snakes. In: Pattern Recognition, 2000. Proceedings. 15th International Conference on. vol. 4, pp. 563–566 vol.4 (2000)
4. Cootes, T.F., Taylor, C.J., Cooper, D.H., Graham, J.: Active shape models – their training and application. Comput. Vis. Image Underst. 61(1), 38–59 (Jan 1995)
5. Delmas, C., Berger, M.O., Kerrien, E., Riddell, C., Trousset, Y., Anxionnat, R., Bracard, S.: Three-dimensional curvilinear device reconstruction from two fluoroscopic views (2015)
6. Eitel, C., Hindricks, G., Dagres, N., Sommer, P., Piorkowski, C.: Ensite velocity cardiac mapping system: a new platform for 3d mapping of cardiac arrhythmias. Expert Review of Medical Devices 7(2), 185–192 (2010), http://www.tandfonline.com/doi/abs/10.1586/erd.10.1
7. Frangi, A., Niessen, W., Vincken, K., Viergever, M.: Multiscale vessel enhancement filtering. In: Wells, W., Colchester, A., Delp, S. (eds.) Medical Image Computing and Computer-Assisted Interventation -MICCAI'98, Lecture Notes in Computer Science, vol. 1496, pp. 130–137. Springer Berlin Heidelberg (1998)
8. Hartley, R.I., Sturm, P.: Triangulation. Computer Vision and Image Understanding 68(2), 146 – 157 (1997)
9. Hoffmann, M., Brost, A., Jakob, C., Bourier, F., Koch, M., Kurzidim, K., Hornegger, J., Strobel, N.: Semi-Automatic Catheter Reconstruction from Two Views. In: Ayache, N., Delingette, H., Golland, P., Mori, K. (eds.) MICCAI 2012, Part I. pp. 584–591. Lecture Notes in Computer Science, Berlin, Heidelberg (2012)
10. Lindeberg, T.: Feature detection with automatic scale selection. International Journal of Computer Vision 30(2), 79–116 (1998)
11. Narayan, S.M., Krummen, D.E., Shivkumar, K., Clopton, P., Rappel, W.J., Miller, J.M.: Treatment of atrial fibrillation by the ablation of localized sourcesconfirm (conventional ablation for atrial fibrillation with or without focal impulse and rotor modulation) trial. Journal of the American College of Cardiology 60(7), 628–636 (2012)
12. Steger, C.: An unbiased detector of curvilinear structures. Pattern Analysis and Machine Intelligence, IEEE Transactions on 20(2), 113–125 (Feb 1998)